Published by :
http://www.ijert.org

International Journal of Engineering Research & Technology (IJERT)
ISSN: 2278-0181
Vol. 5 Issue 12, December-2016

Development of Alternative Fast Simulation Model and Validation of Back-Back Voltage Source Inverter

Peter O. Ohiero
School of Engineering
University of Glasgow, UK

Calum Cossar
School of Engineering
University of Glasgow, UK

Joseph Melone
Power Networks Demonstration
Centre, University of Strathclyde, UK

***Abstract* — This paper presents an alternative modelling method for a full scale back-back voltage source inverter that results in a significant reduction in simulation run time of pulse width modulation voltage source inverters. The proposed modelling method is analytically developed based on control strategy and switching function of voltage source inverter to estimate the 'average' voltage in each switching period across each phase of the voltage source inverter. The average voltage is then used as piecewise linear voltage sources for each phase of alternating current load or electrical machine connected to the voltage source inverter. The developed model was applied to simulation of full scale voltage source inverter with variable speed permanent magnet synchronous generator wind energy conversion systems. A simplified control technique is developed to track maximum power points at the generator side and maintained constant DC voltage at the AC load/grid side using sinusoidal PI current control. The switching model and the proposed average value model of voltage source inverter with PMSG wind energy conversion system have been implemented in the PORTUNUS simulation package. Simulation results of the proposed average value model, switching model and experimental emulator for a small 1kW permanent magnet synchronous generator wind energy conversion systems were compared. The results shows excellent agreement of the average voltage model with the switching model and experimental results over the complete operating range, but with the simulation run time of the proposed average value model being typically 54 times faster than the switching model and thus greatly improves the analysis of wind turbine generator and control technique design process.**

Keywords—Voltage source inverter, Average value model, control strategy

I. INTRODUCTION

Over the years, modelling and simulation have been used to analyze the performance and interaction of voltage source inverter (VSI), electrical machines, and control strategies in different applications such as variable speed drives, solar power systems, wind energy conversion and ocean energy conversion systems. The most widely used simulation model of voltage source inverter is the detailed switching model [1]-[4]. In the detailed switching model, the voltage source converter switches such as transistors and diodes, their switching operation and control strategy are adequately represented in simulation software such as MATLAB/Simulink, LabView, PSCAD, PORTUNUS, etc. However simulation of detailed switching model of voltage source inverter results to long simulation run time. This is because the voltage source inverter devices operate in switch mode and the small time step required by the resolution of PWM control strategies. Another modelling method, the average value model has been widely developed and reported in the literature [5]-[7]. In this approach, average value model is used to replace the VSI switching network in order to eliminate the switch mode operation and speed up simulation run time. The average value model is based on state space averaging. This modelling approach was developed for direct current (DC) to direct current (DC) converters and can be expanded for a three phase VSI, which involves modelling the DC side of the inverter as a current source and the AC side as a voltage source. This paper presents a simple average value model (AVM) of a back-back pulse width modulation (PWM) voltage source inverter which allows fast and accurate simulation and performance analysis of a grid connected renewable energy conversion system. This modelling approach is based on control strategy, switching function and using the duty cycles from the control strategy to analytically average phase voltage in one switching period and then uses the average voltages as a piece-wise linear function to drive voltage sources connected to the terminals of the three-phase permanent magnet synchronous magnet generator (PMSG) or any three-phase system. The developed model is fast to simulate and simple to derive. It can be applied to any three-phase VSI fed system for control and design performance analysis under different operating conditions. However, it cannot be used to investigate the internal dynamics of the VSI. The rest of this paper is organized as follows: Section II discusses the detailed switching model of VSI with variable speed PMSG wind energy conversion systems. Section III introduces the proposed Average value model (AVM) of back-back VSI and its application to simulate variable speed PMSG wind energy conversion system. It also discusses the voltage source inverter loss modelling required to be incorporated into the AVM for the simulation and analysis of power, losses and efficiency of the wind energy conversion system (WECS). Section III also presents the calculation of timing variables required for the estimation of the average phase voltage and DC link voltage modelling, which established a connection between the Generator sides AVM with the AC load side AVM. Section IV presents modelling of wind turbine while section V illustrates the control structure applied at the generator and the AC load side switching and AVM of the WECs. Section VI presents the development of laboratory

International Journal of Engineering Research & Technology (IJERT)
ISSN: 2278-0181
Vol. 5 Issue 12, December-2016

wind energy conversion emulation system which results are used to validate the performance accuracy of the AVM. In Section VII, simulation and experimental results are presented, to demonstrate the performance accuracy of AVM for VSI in a variable speed PMSG wind energy conversion system (WECS) and the effectiveness of the proposed AVM to simulate and analyse maximum power point control strategy of typical WECS. Section VIII draws the conclusion of the paper.

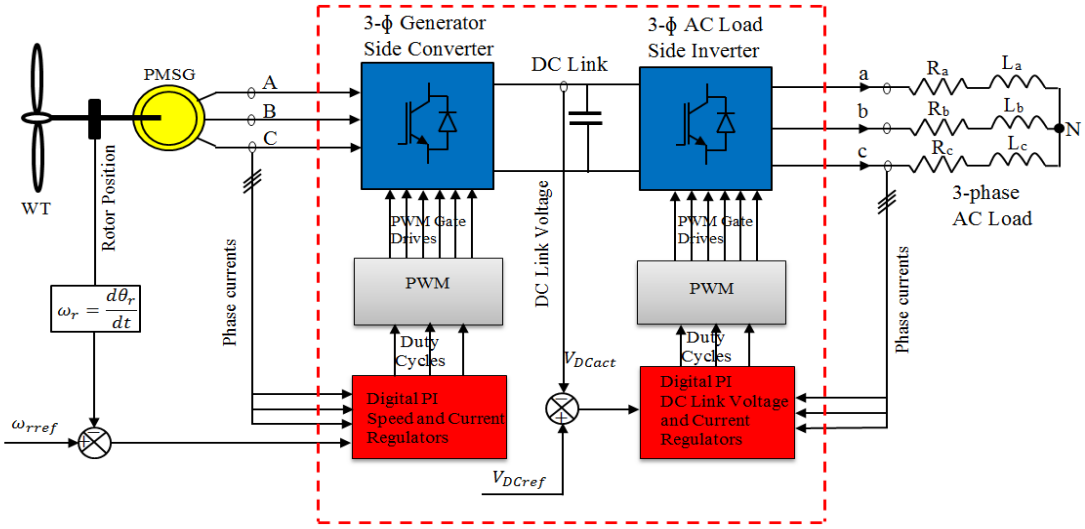

Figure 1 Block diagram of switching model of three phase back-back voltage source converter with variable speed PMSG and wind turbine

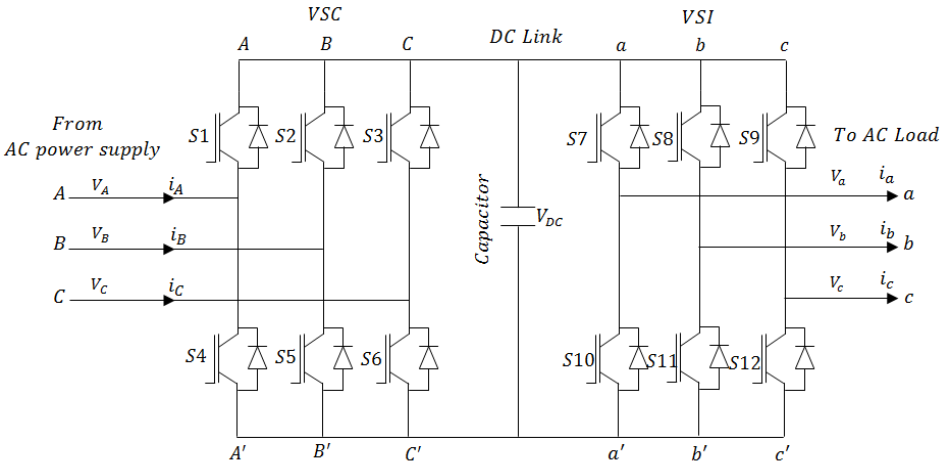

Figure 2 Circuit diagrams of three phase back-to-back voltage source converters

II. DETAILED SWITCHING MODEL OF FULL SCALE BACK-TO-BACK VOLTAGE SOURCE INVERTER

The block diagram of the detailed switching model of a three phase back-back voltage source inverter modelled in this paper is shown in Figure 1. It consists of two sets of three phase voltage source inverters connected back to back to each other. The circuit diagram of the same three phase back – back voltage source inverter is also shown in Figure 2. It is made up of two level, six power electronic converter switches (e.g. insulated gate bipolar transistors, IGBTs) and six antiparallel diodes at the generator side and the same combination at the load/grid side. This configuration is suitable for applications such as grid connected renewable energy source such as wind, ocean and adjustable speed drives.

A. The Generator Side Voltage Source Inverter

The generator side voltage source converter is connected to the AC load/grid side voltage source inverter through a DC capacitor. The DC capacitor serves to filter ripple and provide storage and voltage for the load/grid side inverter. Under the action of the control strategy, the generator side converter converts AC voltages to DC voltage. For the conversion to take place, the two complementary power switches (e.g. S1 and S4) in each phase leg operate in switch mode i.e. when the upper switch on one phase leg is ON, the lower switch on the same phase leg is OFF and vice versa given by

$$S_i = \begin{cases} 1 \text{ upper switch ON} \\ 0 \text{ lower switch OFF} \end{cases}$$

International Journal of Engineering Research & Technology (IJERT)
ISSN: 2278-0181
Vol. 5 Issue 12, December-2016

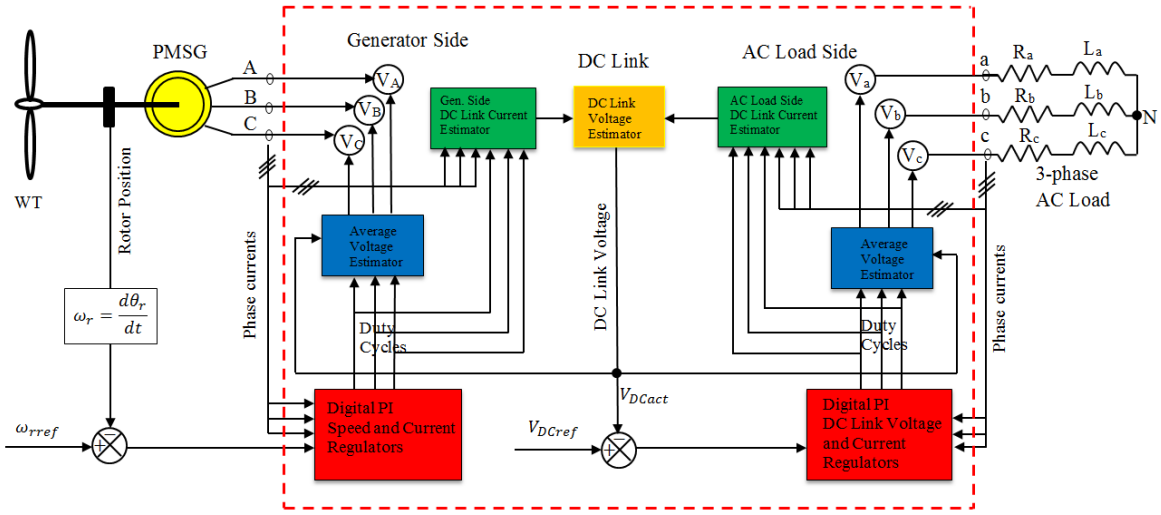

Figure 3: The proposed Average Value Model of three phase back-back voltage source converters with variable speed PMSG and wind turbine

In order to control the switches as stated above, it requires a control strategy. Several control strategies [8]-[11] are available where choices can be made. However, for the purpose of simplicity and the fact that independent voltage sources is required for each phase of the average value model, the sinusoidal pulse width modulation (SPWM) control technique is selected and applied to control the operation of the voltage source converter switches. Figure 2 shows the circuit diagram for a three-phase back-to-back voltage source converter with two transistor (IGBTs) plus anti-parallel diodes in each phase leg. To control the switches, the triangular carrier waveform is compared with the desired sinusoidal waveform to generate the switching signals for each phase leg of the three-phase AC/DC VSI, therefore the three phase voltages at the generator terminals are given as a factor of DC link voltage and switching functions as

$$V_A = \frac{V_{DC}}{3}(2S_A - S_B - S_C) \quad (1)$$

$$V_B = \frac{V_{DC}}{3}(-S_A + 2S_B - S_C) \quad (2)$$

$$V_C = \frac{V_{DC}}{3}(-S_A - S_B + 2S_C) \quad (3)$$

Where V_{DC} is the DC link voltage, S_A, S_B and S_C are the switching function when the upper switch in each phase leg is ON.

B. The Load/grid Side Voltage Source Inverter

The AC load/grid side voltage source inverter of a full scale back-to-back is usually connected to a grid. However for simplicity in this paper it is connected to an isolated AC load. When a control strategy is applied, it converts direct current DC voltage to alternating current voltage. From Figure 1, the configuration of the load side voltage source inverter is the same as that of the generator side; the difference is the mode of conversion. When control strategy is applied, the power converter switches operates and the phase voltages are established at the three phase load connected to the load side inverter and are given by

$$V_a = \frac{V_{DC}}{3}(2S_a - S_b - S_c) \quad (4)$$

$$V_b = \frac{V_{DC}}{3}(-S_a + 2S_b - S_c) \quad (5)$$

$$V_c = \frac{V_{DC}}{3}(-S_a - S_b + 2S_c) \quad (6)$$

Where S_a, S_b *and* S_c are switching functions when the upper switch in each phase's leg at the load side is ON.

III PROPOSED AVERAGE VALUE MODEL OF BACK-TO-BACK VOLTAGE SOURCE INVERTER

The proposed average value model of a back-back voltage source inverter is developed based on the principle of control strategy and switching functions to analytically estimate the 'average' ac voltage across each phase of an electrical machine e.g. PMSG and AC load during each PWM switching period and then using these average voltages as piecewise-linear voltage sources for each phase of the PMSG and AC load. Figure 3 shows the AVM of a two level three-phase back-back VSI. The VSI is totally eliminated and replaced with an analytical model and three-phase voltage sources driven by the average phase voltage estimates in one switching period.

In order to implement the AVM, the choice of control strategy that is compatible with three-phase system is important. The SPWM is used because it is an independent control technique in which each phase is controlled independent of the other. In SPWM there are three independent proportional integrals (PI). The measured sinusoidal current is compared with the referenced sinusoidal current to produce an error which is processed by the PI regulator to generate the duty cycles. The duty cycles are then used by the AVM to estimate the average phase voltage.

International Journal of Engineering Research & Technology (IJERT)
ISSN: 2278-0181
Vol. 5 Issue 12, December-2016

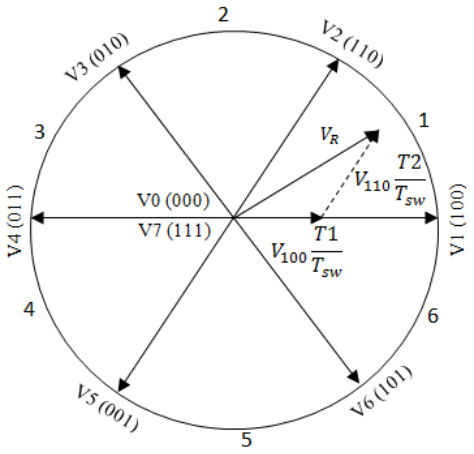

Figure 4 Space voltage vectors and sectors

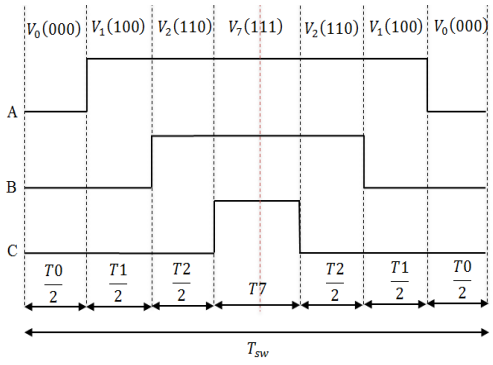

Figure 5: Symmetrical three phase PWM outputs

In order to estimate average voltage in one switching period, the switching state of each phase leg of voltage source inverter is utilized. There are two switching states in each phase leg of a VSI. For a three-phase system there are a total of 2^3 = 8 switching states resulting in 8 voltage vectors and eight possible circuit arrangement of the three phase PM machine. Six of the voltage vectors are active and two are zero voltage vectors. The voltage vectors are located in six sectors of voltage vector hexagon as shown in Figure 4 [12]. For each of the sectors, there is a resultant voltage vector which can be calculated using the two adjacent voltage vectors and two zero voltage vectors. For sector 1, the resultant voltage vector is given by (7) and the switching time given by (8).

$$V_R = \frac{T1V1}{T_{sw}} + \frac{T2V2}{T_{sw}} + \frac{T0V0}{T_{sw}} + \frac{T7V7}{T_{sw}} \quad (7)$$

$$T_{sw} = T1 + T2 + T0 + T7 \quad (8)$$

Where, V_R is the resultant voltage vector, T_{sw} switching period, $T1$ *and* $T2$ are the time intervals of the active voltage vectors, $T0$ and $T7$ are the time interval of the zero voltage vectors. The zero voltage vectors, $V0$ and $V7$ are approximated to zero, therefore equation (7) becomes:

$$V_R = \frac{T1V1(100)}{T_{sw}} + \frac{T1V2(110)}{T_{sw}} \quad (9)$$

The average voltage estimation depends on the sector in which the resultant voltage vector resides during the switching cycle. Therefore, the first step is to accurately determine the sector to estimate the average phase voltage. Using the carrier-based sinusoidal PI current control strategy, there are three separate PI current controllers which independently generate duty cycles during the switching period. The duty cycles can be ordered from the largest to smallest. Doing so will result in a permutation of the phase duty cycles; dA, dB, dC. And this results to exactly 6 possible permutations, corresponding to 6 sectors.

A. Calculation of timing variables

To implement equation (9), the time the adjacent voltage vectors in each sector stays connected to the DC link voltage should be calculated. This time depends on the pattern of the PWM output at each commanded duty cycle and as the PWM pattern changes from sector to sector the time also varies from sector to sector.

Considering that the inverter is connected to a permanent magnet synchronous generator in a renewable energy conversion system applications, at each commanded duty cycle, PWM voltage is established at the terminals of the three-phase PMSG and AC Load. For one switching period the PWM voltage is usually symmetrical as shown in Figure 5. It can be seen from Figure 5 that the second half of the PWM waveform is a mirror image of the first half and the switching operation in the first half is repeated in the second half. This makes it possible to simplify the estimation of average phase voltage using half of the symmetry in a complete switching period. Hence, PWM waveform half symmetry is then constructed for six sectors considering only the active voltage vectors as shown in Figure 6 in order to calculate the time of adjacent voltage vectors. Sector 1 is used as an example to illustrate how the average phase voltage is estimated in a switching period. In sector 1, the time $T1$ and $T2$ for the voltage vectors V1 and V2 is known by simply identifying the length of time each of the phases of the three-phase PMSG stay connected to the DC voltage supply. The sequence is to identify and compare the relative lengths of the three duty cycles such as the long, longer and the longest among the three phase PWM waveform in each sector. Figure 7 shows the PWM waveform of the commanded voltage vectors in sector 1, where, Td_A, Td_B, Td_C, are the length of time phase A, B, C stay connected to the positive terminals of the DC voltage supply. With reference to Figure 7, the switching period is divided into four, $T0$, $T1$, $T2$, $T7$ with the matching voltage vectors. From Figure 7, $Td_A > Td_B > Td_C$ therefore, the timing variables in sector 1 are given by;

$$T1 = Td_A - Td_B \quad (10)$$

$$T2 = Td_B - Td_C \quad (11)$$

International Journal of Engineering Research & Technology (IJERT)
ISSN: 2278-0181
Vol. 5 Issue 12, December-2016

Note that this derivation changes dependent on the sector. In order to apply equation (9) to estimate the average voltage over a switching period, calculation must be carried out to estimate the voltage drop across each of the phases as a factor the DC voltage.

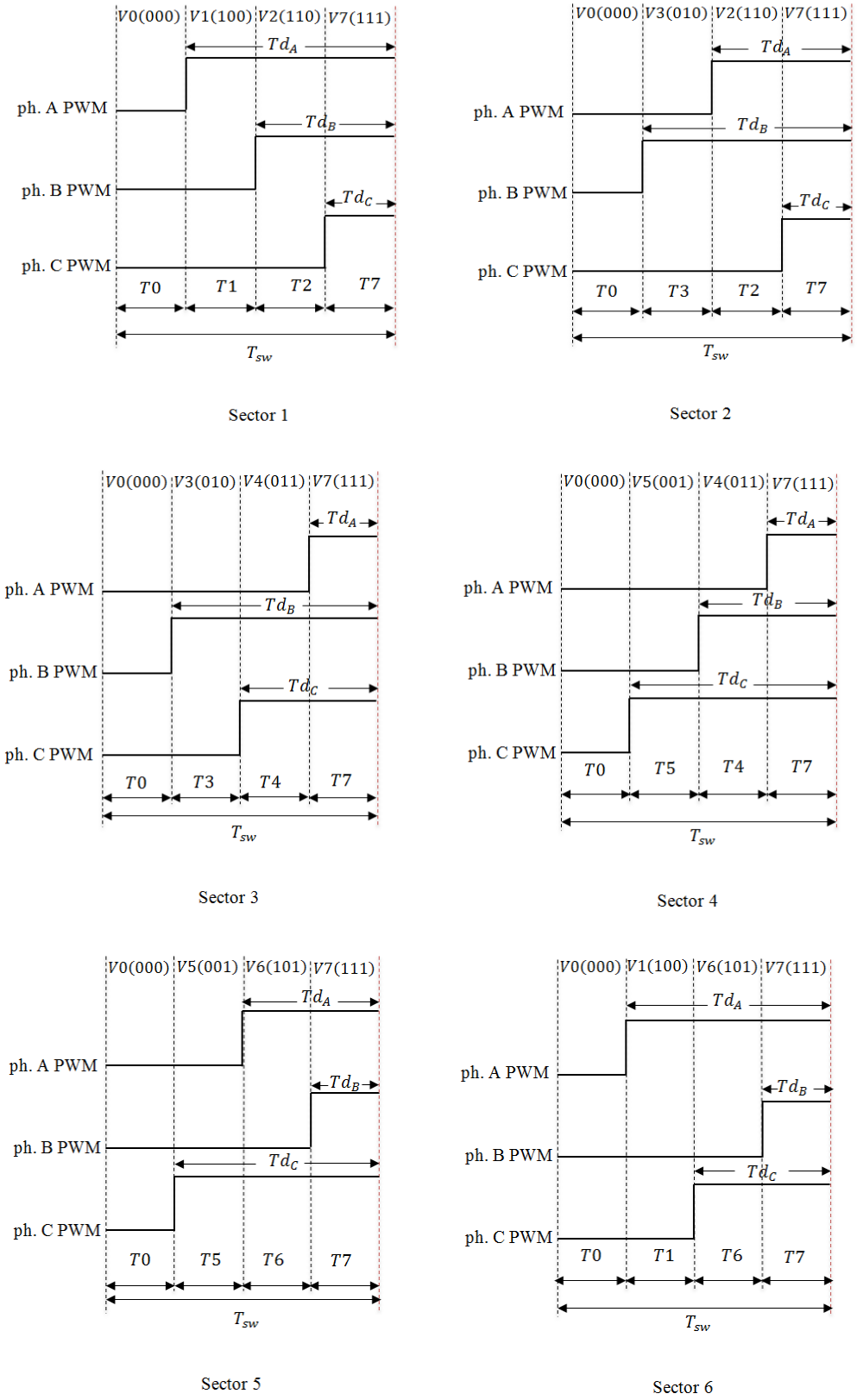

Figure 6 PWM voltage waveform and commanded voltage vectors

International Journal of Engineering Research & Technology (IJERT)
ISSN: 2278-0181
Vol. 5 Issue 12, December-2016

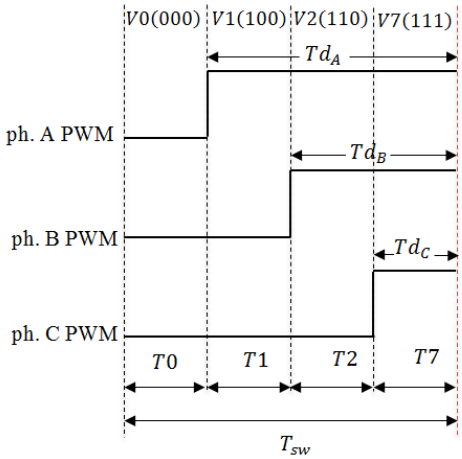

Fig. 7: PWM waveform half symmetry of in sector 1

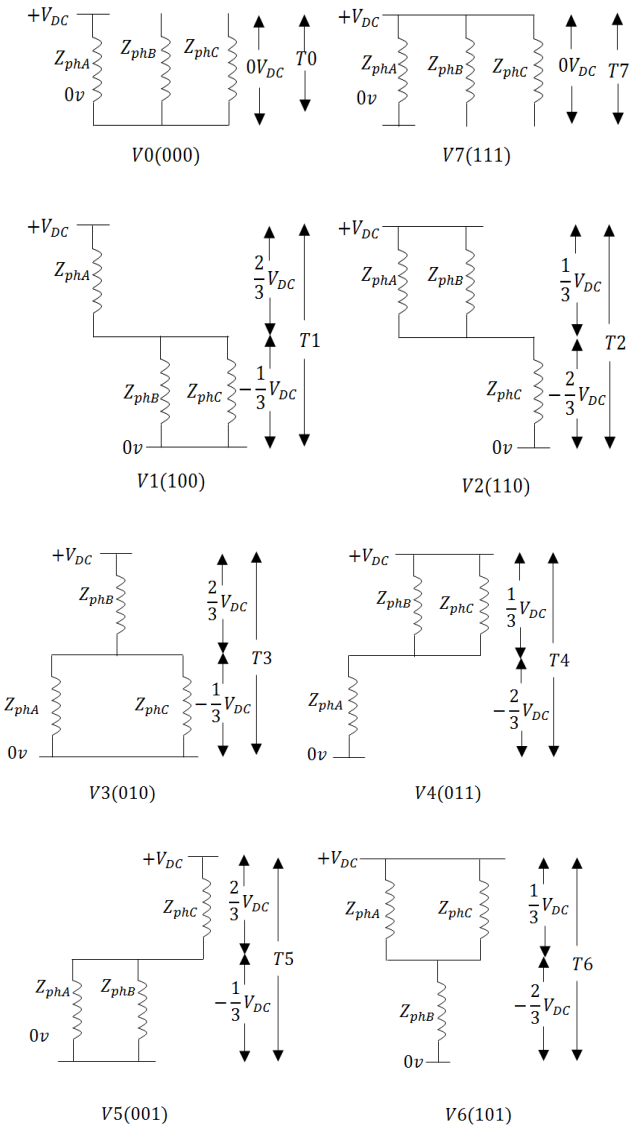

Figure 8 Three phase equivalent circuits of the commanded voltage vector and voltage drop across phases

This can be achieved by forming equivalent circuits resulting from the commanded eight voltage vectors due to the eight switching combinations of the voltage source inverter in a switching period as shown in Figure 8. In each of the equivalent circuits, the DC voltage forms a series circuit with the three-phase PMSG winding and AC load/grid represented by R-L configuration. Therefore, the voltage drop across each phase e.g. V_A, V_B and V_C can be calculated from DC voltage using the Voltage Divider Rule given as

$$V_k = \frac{Z_k}{Z_T} V_{DC} \qquad k \in (A, B, C) \tag{12}$$

Where; V_k is the voltage drop across the phases; A, B, C, Z_T is the total impedance of the series circuit, Z_k is the impedance across the phase in which the voltage drop is calculated and V_{DC} is the DC supply voltage. Equation (12) is used to calculate the voltage drop across each of the phases due to the DC voltage in each of the sectors. For sector 1, the equivalent circuits for voltage vectors V1 (100), V2 (110), V0 (000) and V7 (111) are used as shown in Figure 8. Substituting (10) and (11) into (9) and using the equivalent circuits of the three-phase PMSG or three phase AC system as a results of the commanded voltage vector in sector 1 shown in Fig 7, and considering only the active voltage vectors, the voltages V1 (100) and V2 (110) are replaced with their corresponding voltage drop due to V_{DC} and the average voltage for the three phases in sector 1 are given as;

$$V_{Aavg} = \frac{\frac{2}{3}V_{DC}T1 + \frac{1}{3}V_{DC}T2}{T_{sw}} \tag{13}$$

$$V_{Bavg} = \frac{-\frac{1}{3}V_{DC}T1 + \frac{1}{3}V_{DC}T2}{T_{sw}} \tag{14}$$

$$V_{Cavg} = \frac{-\frac{1}{3}V_{DC}T1 - \frac{2}{3}V_{DC}T2}{T_{sw}} \tag{15}$$

V_{Aavg} , V_{Bavg}, V_{Cavg} are the average voltage in phase A, B and

The average voltage estimation modelling approach calculates the average phase voltage in every sector in a switching period independently per phase given a total of three sets of equations for each sector. This derivation relies strongly on the combination of equivalent circuit diagrams of the commanded voltage vectors and the PWM waveform half symmetry in each sector. Therefore, in a similar process, the average voltages in the other sectors are estimated and the results are shown in Table 1. Therefore, the total average voltage per phase is the sum of the voltage estimated in all the sectors per phase. This total average voltage per phase is then use to drive each of the voltage sources connected to the three-phase PMSG, three phase AC load and can also be used with any three phase system where control is required. The difference is that the duty cycles for the load/grid side AVM depends on the AC load side control strategy. In each switching interval, this calculation requires knowledge of the DC voltage value V_{DC} and switching period T_{SW} (this depends on the switching frequency chosen). In this paper the value used for the switching frequency is 20 kHz and this corresponds to a switching period of 50μs.

International Journal of Engineering Research & Technology (IJERT)
ISSN: 2278-0181
Vol. 5 Issue 12, December-2016

Table 1: Summary of average voltage estimation per phase for each sector

Sectors	Commanded duty cycles configuration	Timing calculation	Average estimated voltage		
			V_A	V_B	V_C
1	$Td_A \geq Td_B$ $Td_B \geq Td_C$ $Td_A \geq Td_C$	$T1 = Td_A - Td_B$ $T2 = Td_B - Td_C$	$\frac{V_{DC}}{3T_{sw}}(2T1 + T2)$	$\frac{V_{DC}}{3T_{sw}}(-T1 + T2)$	$\frac{V_{DC}}{3T_{sw}}(-T1 - 2T2)$
2	$Td_B \geq Td_A$ $Td_A \geq Td_C$ $Td_B \geq Td_C$	$T2 = Td_A - Td_C$ $T3 = Td_B - Td_A$	$\frac{V_{DC}}{3T_{sw}}(T2 - T3)$	$\frac{V_{DC}}{3T_{sw}}(T2 + 2T3)$	$\frac{V_{DC}}{3T_{sw}}(-2T2 - T3)$
3	$Td_B \geq Td_C$ $Td_C \geq Td_A$ $Td_B \geq Td_A$	$T3 = Td_B - Td_C$ $T4 = Td_C - Td_A$	$\frac{V_{DC}}{3T_{sw}}(-T3 - 2T4)$	$\frac{V_{DC}}{3T_{sw}}(2T3 + T4)$	$\frac{V_{DC}}{3T_{sw}}(-T3 + T4)$
4	$Td_C \geq Td_B$ $Td_B \geq Td_A$ $Td_C \geq Td_A$	$T4 = Td_B - Td_A$ $T5 = Td_C - Td_B$	$\frac{V_{DC}}{3T_{sw}}(-2T4 - T5)$	$\frac{V_{DC}}{3T_{sw}}(T4 - T5)$	$\frac{V_{DC}}{3T_{sw}}(T4 + 2T5)$
5	$Td_C \geq Td_A$ $Td_A \geq Td_B$ $Td_C \geq Td_B$	$T5 = Td_C - Td_A$ $T6 = Td_A - Td_B$	$\frac{V_{DC}}{3T_{sw}}(-T5 + T6)$	$\frac{V_{DC}}{3T_{sw}}(-T5 - 2T6)$	$\frac{V_{DC}}{3T_{sw}}(2T5 + T6)$
6	$Td_A \geq Td_C$ $Td_C \geq Td_B$ $Td_A \geq Td_B$	$T1 = Td_A - Td_C$ $T6 = Td_C - Td_B$	$\frac{V_{DC}}{3T_{sw}}(2T1 + T6)$	$\frac{V_{DC}}{3T_{sw}}(-T1 - 2T6)$	$\frac{V_{DC}}{3T_{sw}}(-T1 + T6)$

International Journal of Engineering Research & Technology (IJERT)
ISSN: 2278-0181
Vol. 5 Issue 12, December-2016

Applying the average voltage the, average instantaneous current can be written as

$$\frac{di_A}{dt} = \frac{V_{Aavg} - i_A R}{L} \quad (16)$$

$$\frac{di_B}{dt} = \frac{V_{Bavg} - i_B R}{L} \quad (17)$$

$$\frac{di_C}{dt} = \frac{V_{Cavg} - i_C R}{L} \quad (18)$$

And the developed electromagnetic torque is given as function of the rotor natural flux amplitude and the stator currents in three-phase PMSM as follows

$$T_e = p\varphi_m(i_A + i_B + i_C) \quad (19)$$

$$T_e = p\varphi_m I_m \quad (20)$$

B. Modelling of DC Link Voltage

Modelling the DC link voltage is important in order to implement the generator and AC load side AVM. The DC link model provides the required value of the DC link voltage and also establishes a 'Virtual' connection between the variable speed generator output and AC load/grid. The DC link voltage model is developed based on the generator side DC link current and the AC load/grid side DC link current as well as the DC link capacitance value. The generator side DC link current is determined using the PWM switching pattern, the equivalent circuits and associated switch states shown in Figure 5 – Figure 8. An example of how the generator side DC link current in sector 1 is estimated is given. Each sectors is divided into four, for example in sector 1, there are four divisions each having times T0, T1, T2 and T7 in which the phases stay connected to the positive terminals of the DC link voltage. During the states T0 and T7 all the phase currents are circulating around the phases and therefore the DC Link current is zero during these times. During state T1 the DC Link current is equal to the phase A current and during state T2 the DC Link current is equal to the negative of phase C current, therefore the average DC Link current during this switching period in sector 1 is given as follows:

$$I_{DC_{gen}} = \frac{T1}{Tsw} i_{phA} - \frac{T2}{Tsw} i_{phC} \quad (21)$$

In a similar way, the AC load/grid side is modelled as a balanced three phase AC load consisting of a series combination of resistance and inductance. PWM outputs and equivalent circuits in sector 1 are similar to the one shown in Figure 5- Figure 7 and is used to derive the DC Link current. For ease in identification of the parameters used for the estimation, the three-phase designations used for the AC load side are a, b, c. Once again a similar approach is adopted on the load/grid side to determine 'instantaneous' DC Link current supplied to the load given by

$$I_{DC_{load}} = \frac{T1}{Tsw} i_{pha} - \frac{T2}{Tsw} i_{phc} \quad (22)$$

The DC link currents in (21) and (22) are calculated in all the sectors in a switching period and averaged over a period of time to obtain the actual DC link current. The final step is to determine the 'instantaneous' DC link voltage which is achieved through the relationship:

$$V_{DC} = \frac{1}{C}\int(\sum_{n=1}^{6} I_{DC_{gen}} - \sum_{n=1}^{6} I_{DC_{load}}) \quad (23)$$

Where n is the number of sectors

Hence, the DC link voltage can be modelled as parallel current sources separated by a DC link capacitor where the average DC current estimations are then input to a piecewise linear current source which then represents the 'instantaneous' DC Link current supplied by the generator, $I_{DC_{gen}}$ and that supplied to the AC load inverter, $I_{DC_{load}}$. The DC link voltage can also be determined online estimation of knowing the equivalent value of the DC link capacitor.

C. Voltage Source Inverter Loss Modelling

Since the voltage source inverter switching network is totally absent in the proposed AVM and in order to predict accurate power flow and output at different points of the WECS, the VSI losses are modelled and incorporated into the AVM of the WECS. The voltage source inverter losses depend on the current that flows, the voltage, the control strategy and the operating condition. The voltage source inverters losses consist of conduction and switching losses and are calculated for one phase of the inverter consisting of an IGBT and a diode and the result multiplied by the number of combination of IGBT and diode to obtain total losses for three phases using the manufacturer data sheet approach. The conduction losses for one IGBT and diode are given by [13];

$$P_{condIGBT} = V_{CE0} i_m \left(\frac{1}{2\pi} + \frac{m\cos\emptyset}{8}\right) + i^2{}_m r_C \left(\frac{1}{8} + \frac{m\cos\emptyset}{3\pi}\right) \quad (24)$$

$$P_{condDiode} = V_{D0} i_m \left(\frac{1}{2\pi} - \frac{m\cos\emptyset}{8}\right) + i^2{}_m r_D \left(\frac{1}{8} - \frac{m\cos\emptyset}{3\pi}\right) \quad (25)$$

$$i_m = \sqrt{2}\, i_{rms}$$

Where, $i_m = \sqrt{2}\, i_{rms}$ is the peak value of the input current
m is the modulation index
$\emptyset$ is the phase angle
$\cos\emptyset$ is power factor (pf)

The switching losses in the IGBTs over a switching cycle depends on the switching frequency and the turn-on and turn-off energies given as

$$P_{swIGBT} = (E_{onIGBT} + E_{offIGBT}) f_{sw} \quad (26)$$

For the diode, the reverse recovery energy from which the switching losses in the diode is calculated is given as

$$E_{onDiode} = \int_0^{t_1} V_D(t) + i_D(t)dt \quad (27)$$

$$E_{onDiode} = \frac{1}{4} Q_{rr} V_{Drr} \quad (28)$$

International Journal of Engineering Research & Technology (IJERT)
ISSN: 2278-0181
Vol. 5 Issue 12, December-2016

Thus the diode switching losses can be calculated as

$$P_{swDiode} = (E_{onDiode})f_{sw} \quad (29)$$

Where, Q_{rr} is the diode recovery charge, V_{Drr} the reverse recovery voltage across the diode and f_{sw} is the control strategy switching frequency. Calculating the switching losses in IGBTs and diode is usually a difficult task. The simplest approach is the use of datasheet values. The threshold voltage across the IGBT, V_{CE0}, diode, V_{D0}, the on-state resistance of the IGBT r_{CE} and diode r_D are obtained from the output characteristics of the power electronic devices and the turn-on and turn-off energies
as a function of IGBTs and diode current, Q_{rr} and V_{Drr} that can are obtained from the datasheet of the power electronic converter while the displacement factor, m and power factor, $\cos\emptyset$ are usually obtained from the nameplate of the machine under investigation.

IV. MODELLING OF WIND TURBINE

The mechanical power output of the wind turbine is calculated using the generic equation given as follows [14][15];

$$P_m = 0.5\rho A C_p(\lambda, \beta){V_w}^3 \quad (30)$$

Where: ρ is the air density (1.225kg/m^2), A is the swept area ($A = \pi R^2$) of the rotor blade, C_p is the power (performance) coefficient of the wind turbine, λ is the tip-speed ratio, β is the rotor blade pitch angle and V_w is the wind speed (m/s).
It can be seen that mechanical power of the wind turbine, P_m depends on the aerodynamic characteristics of the wind turbine defined by the efficiency of the wind turbine called the power coefficient, C_p. The power coefficient C_p is a nonlinear function of the tip speed ratio and the pitch angle with the maximum limit set by Betz limit as $C_p = \frac{16}{27} = 0.593$ [16]. For fixed-pitch angle blade, the pitch angle, $\beta = 0$ therefore, the actual mechanical power extracted from the wind by the fixed-pitch angle blade of the wind turbine can be calculated by

$$P_m = 0.5\rho\pi R^2 C_p(\lambda){V_w}^3 \quad (31)$$

In this case, the power coefficient, C_p depends only on the tip-speed ratio given as

$$\lambda = \frac{\omega_r R}{V_w} \quad (32)$$

Where: ω_r is the wind turbine rotor angular speed, R is the wind turbine blade radius
In order to generate electrical power, the mechanical power extracted from the wind turbine described in (30) must apply mechanical torque on the generator. The mechanical torque is given by

$$T_m = \frac{P_m}{\omega_r} \quad (33)$$

Combining (31) and (32) and substitute into (33), the mechanical torque can be calculated using the expression

$$T_m = 0.5\rho\pi R^3 {V_w}^2 C_t \quad (34)$$

$$C_t = \frac{C_p(\lambda)}{\lambda} \quad (35)$$

Where: T_m is the mechanical torque (Nm) and C_t is the torque coefficient.

The mechanical torque produce by the wind turbine further interact with the electromagnetic torque to generate electricity. This is represented by

$$\frac{d\omega_r}{dt} = \frac{1}{J}(T_m - T_e + B\omega_r) \quad (36)$$

Where J is the combine wind turbine rotor and generator inertia, ω_r is the turbine rotational speed (rad/sec), B is the viscous friction coefficient, T_m and T_e are the turbine mechanical and generator electrical torque respectively. Therefore equations 31-34 are used to model the wind turbine and connected to the PMSG model.

V. CONTROL STRATEGY STRUCTURE

The proposed AVM of back-back voltage source inverter is applied to simulate variable speed PMSG wind energy conversion system. Figure 9 and Figure 10 show the control structure for the PMSG WECS. It consists of the Generator side controller and the AC load/grid side controller. The generator side controller controls the operation of the PMSG to track the maximum power point at different wind speeds and the AC load side controller ensures the DC link voltage is maintained constant to enable power to be accurately transferred to the AC load or grid.

International Journal of Engineering Research & Technology (IJERT)
ISSN: 2278-0181
Vol. 5 Issue 12, December-2016

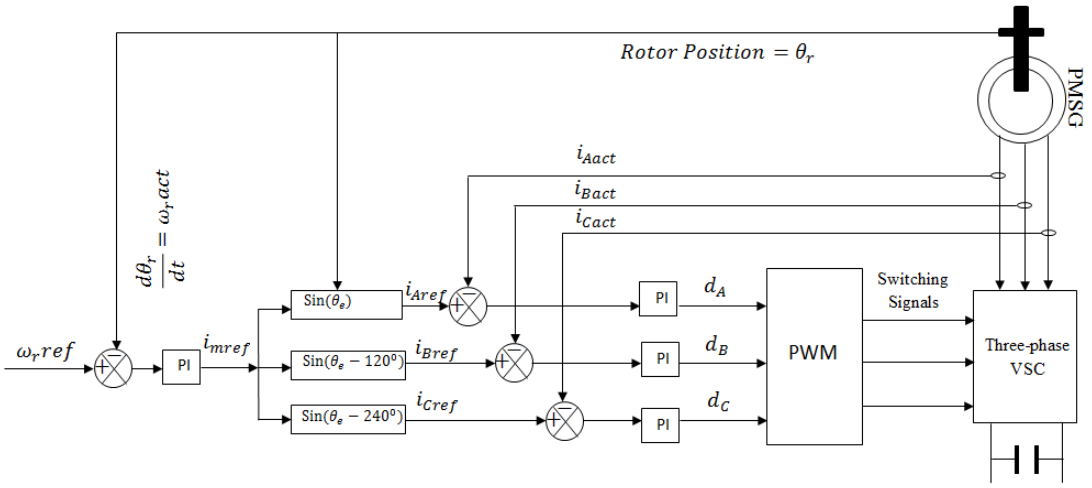

Figure 9 Generator side control technique structure

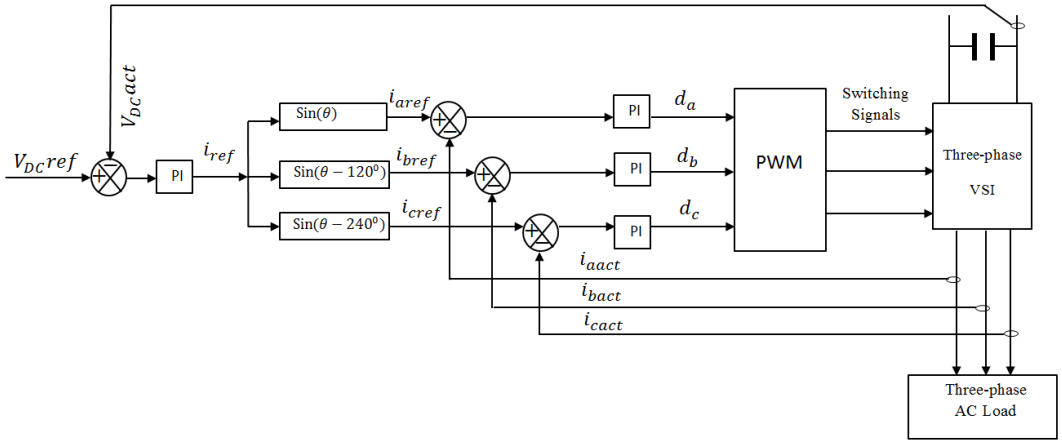

Figure 10 AC Load side control technique structure

To maximise the WECS power output, the generator side controller controls the PMSG speed and torque by controlling the stator current to its reference value in order to track maximum power points below rated speed and above rated speed limits power output to rated value. This is based on the fact that for every wind speed, there is an optimum (reference) rotor speed and stator current (torque) demand at which power generated is at its maximum. Speed is controlled when the PMSG produces torque opposite to the mechanical torque given as;

$$T_e = -(K_T {\omega_r}^2 - B\omega_r) \tag{37}$$

$$K_T = 0.5\rho\pi C_p max(\frac{R}{\lambda_{opt}})^3 \tag{38}$$

Therefore, equation (37) is used to calculate the current reference for the generator side as follows:

$$i_m = \frac{T_e}{K_t} \tag{39}$$

Where i_m is the peak value of the sinusoidal reference current, K_t is the torque constant of the PMSG given by $K_t = \frac{3}{2}p\phi_m$ and p is the number of pole pairs, ϕ_m is the magnetic flux. Both the generator and AC load control have an inner current control loop. For the generator side controller to control the PMSG current, a current reference is required. This is usually obtained by processing the speed error from the comparison of the measured rotor speed and reference rotor speed [17]. However, to simplify control technique to track maximum power points, the reference rotor speed can be set as a function of each phase current reference for different wind speed using look-up table. As wind speed varies, the actual rotor speed is measured and fed into the look-up table and a matching reference currents is selected. The current control loop then compares the reference current with the measured (actual) current and ensures that the profile of the reference current is tracked by the measured current. Current sensors are used to measure the phase current per phase, i_{Aact}, i_{Bact}, i_{Cact} and compares with the sinusoidal current reference, i_{Aref}, i_{Bref}, i_{Cref} to generate current errors. The current errors are fed into the relevant PI regulator. For the switching model, the outputs of the PI regulators are compared with a triangular carrier signal and modulated at a high frequency (e.g. 20kHz as used in the models) to generates complementary gate drive signals in the relevant phase-leg while for the AVEM, the outputs of the PI regulators are used to estimate the average voltages per phase and applies the

International Journal of Engineering Research & Technology (IJERT)
ISSN: 2278-0181
Vol. 5 Issue 12, December-2016

average voltages to voltage sources connected to the terminals of the PMSG. The same process applies to the AC load/grid current control loop. However, the current control loop for the AC load/grid controller is fed from the outer DC voltage control loop.

VI. WIND ENERGY CONVERSION EMULATION SYSTEM

In order to validate the performance of the proposed AVM of WECS, a 1kW wind energy conversion system emulator has been developed.

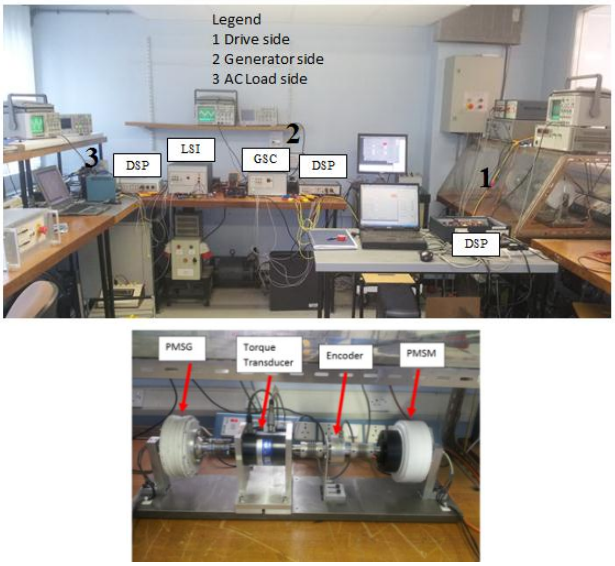

Figure 11 Experimental wind energy conversion emulation systems

Figure 11 shows the picture of the experimental test rig showing the hardware for a PMSG WECS. The PMSM is directly connected to the PMSG which in turn is connected to the three-phase AC load through a three-phase back-back voltage source inverter utilizing IGBTs with antiparallel diodes. The whole set up is developed to emulate a typical WECS. The WECS emulation system uses the rotor shaft speed and wind speed to generate the reference current used to control the PMSM to follow the outline of the Cp/tip speed ratio thereby producing variable speed to the PMSG as the wind speed changes.

VII. RESULTS AND DISCUSSION

The detailed switching model and the proposed AVM of a three phase back – back voltage source inverter with variable speed PMSG WECS described above are developed and implemented in the PORTUNUS simulation package. Simulation studies and experiments are carried out based on the parameters for the PM machines and wind turbine shown in Appendix A, Table 3 and Table 4. Initial simulations were to verify the ability of the AVM to implement current control and to accurately track the switched model. This is followed by the verification of the steady state performance of wind turbine model and the WECS emulation system and the ability of the AVM to reproduce the prediction of the switching model and experimental wind turbine emulator. To achieve this at each wind speed, the speed of the PMSG is controlled by controlling the phase current and at different rotor speed, the turbine torque and power of the WECS are recorded. The PMSG current control using detailed switching model and AVM are shown in Figure 12 and Figure 13.

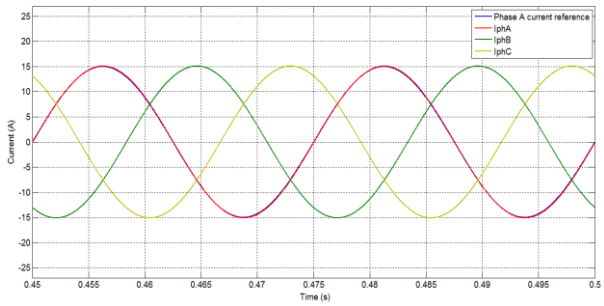

Figure 12 Simulation of PMSG stators current control at 15A reference at 12m/s using AVM

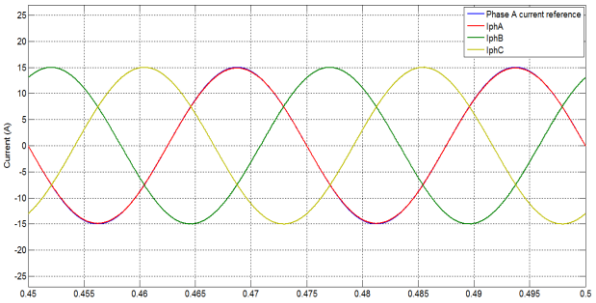

Figure 13 Simulation of PMSG stators current control at 15A reference at 12m/s using detailed switching model.

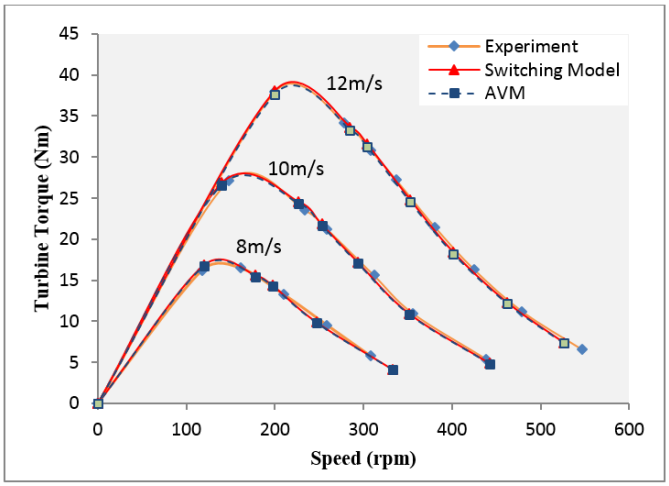

Figure 14 Comparison of wind turbine torque using AVM, switching model and experiment

International Journal of Engineering Research & Technology (IJERT)
ISSN: 2278-0181
Vol. 5 Issue 12, December-2016

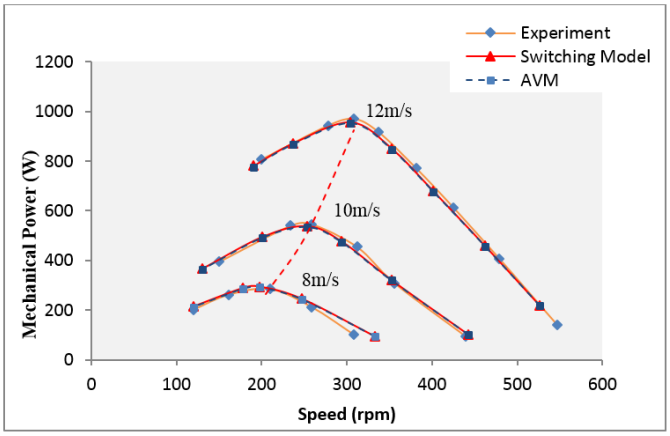

Figure 15 Comparison of wind turbine power versus rotor speed using AVM, switching model and experiment

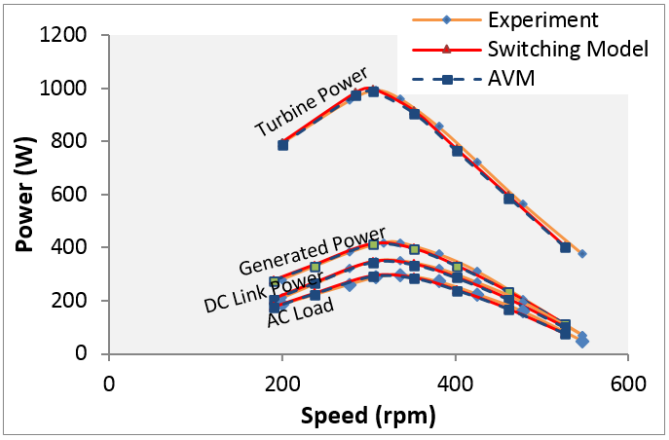

Figure 16 Power flow versus speed comparison of WECS using AVM, switching model and experiment at 12m/s

From Figure 12 and Figure 13 it can be seen that the AVM successfully implemented current control predicting the same results as the switching model in tracking the waveform of the reference current, in magnitude and phase sequence. Figure 14 shows the comparison of the turbine torque and Figure 15 shows the comparison turbine power versus speed characteristics. Also Figure 16 shows the comparison power flow from the wind turbine to the AC load at 12m/s. It can be seen that the wind turbine torque and power characteristics of the experiments are accurately reproduced using the detailed switching model and the proposed AVM. Comparing the AVM to the switching model and experiment, the results of the AVM agrees with the switching model without loss of accuracy but there is difference between the results of the simulation models and experiments especially at higher speed region. This is due to the differences in the loss consideration between the models and the experiment. While all the loss components are part of the real time experiment test rig hardware, the simulation models calculate losses based on manufacturers datasheet and it is difficult to accurately compute the correct losses over the complete operating range of the system.

Thereafter, simulations and tests were conducted to verify the performance of the AVM under dynamic situations in implementing MPPT control for variable wind speed input to the AVM and WEC emulation system.

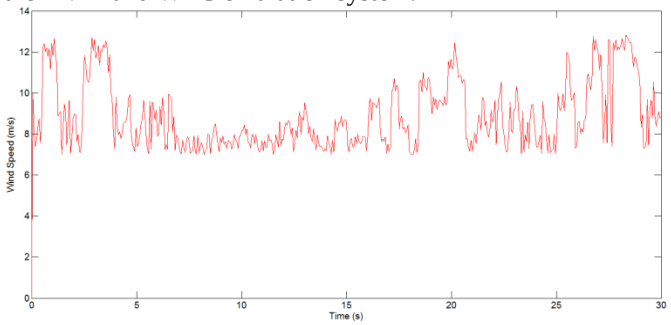

Figure 17 Wind speed profile

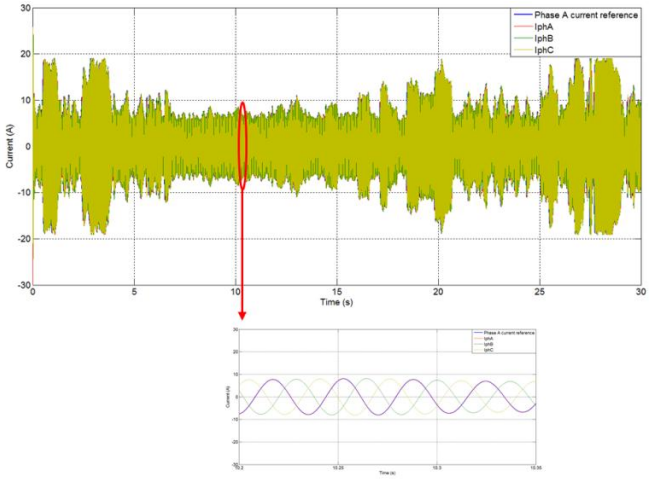

Figure 18 PMSG phase current under MPPT control using AVM

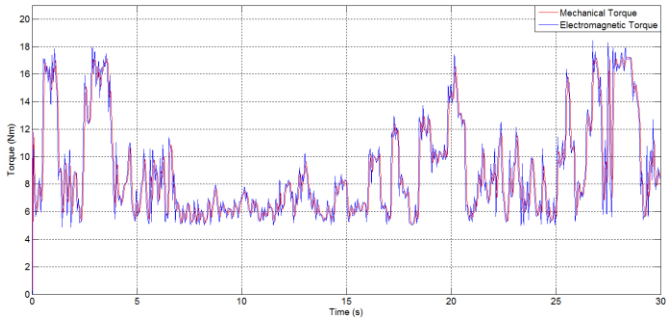

Figure 19 Torque response control using AVM

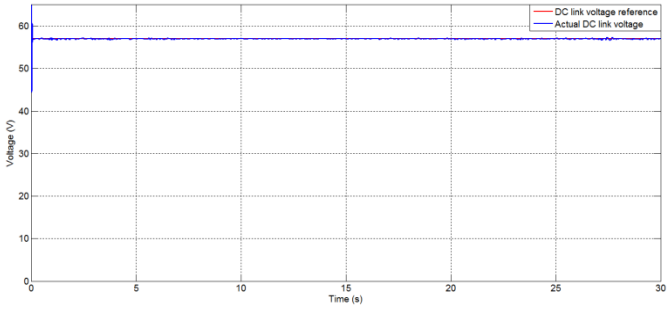

Figure 20 DC link voltage

International Journal of Engineering Research & Technology (IJERT)
ISSN: 2278-0181
Vol. 5 Issue 12, December-2016

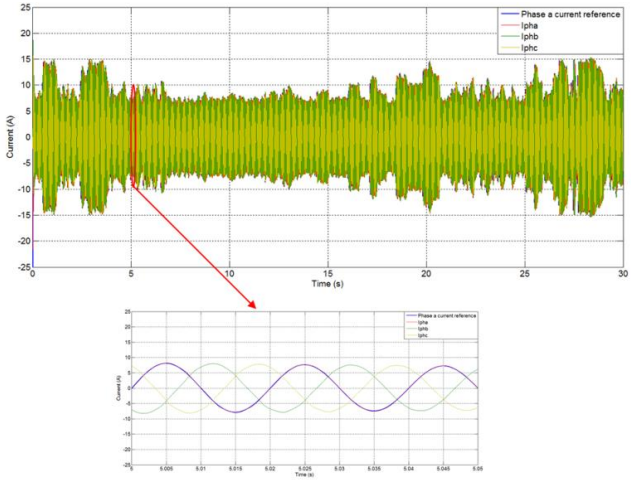

Figure 21 AC Load three phase current

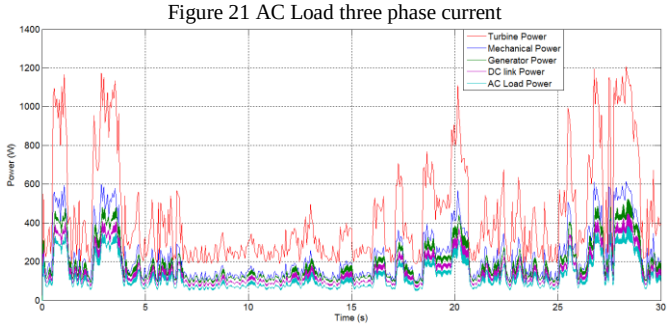

Figure 22 Simulation of WECS power flow from the wind turbine to the AC load

Figure 17 – Figure 22 show the simulation of the dynamic performance of the AVM and its ability to implement control technique to track maximum power as wind speed varies. Figure 17 shows the wind speed profile applied to the model. Figure 18 shows the prediction of the AVM and the dynamic performance of the control technique in which the PMSG phase current is controlled to track the waveform and amplitude of the reference current in order to generate negative electromagnetic torque which balances the mechanical torque and generates maximum power. It can be seen that, the current demand of the generator varies as wind speed varies to track maximum power. The dynamic performance of the control technique in controlling the PMSG phase current to track the waveform of the reference current is shown in the electromagnetic torque as shown in Figure 19. The PMSG generates a negative electromagnetic torque equal in magnitude to the mechanical torque based on equation (37) due to current control establishing a point of equilibrium between the torques where maximum power is extracted. Figure 20 shows the DC link voltage as wind speed varies. Irrespective of the variation in wind speed, between 7m/s and 12m/s, the DC voltage remained constant at the reference value of 57V generating a fixed frequency of 50Hz phase current to the AC load/grid shown by the zoomed section of Figure 21. This is one important requirement of any wind energy conversion system where generated power is required to be utilised by conventional AC loads or connected to the grid. Figure 22 shows the wind energy conversion system power flow. It shows the simulated amount of power that has been extracted from the turbine, generated by the generator and delivered to the AC load as the wind speed varies. The primary aim of the PMSG control technique is to extract as much power as possible from the wind. It can be seen that the when the wind speed varies maximum power at different points of the WECS is tracked. As can be seen from Figure 22, power losses in the voltage source inverters have been considered in the AVM to ensure accurate flow of power from the generator to the AC load/grid. The result shows that, the AVM transfers power accurately from the wind turbine to the AC load/grid.

Figure 23, shows the maximum power points obtained from the simulation of the AVM under the MPPT control technique at various wind speeds. It can be seen that below and up to the rated wind speed of 12m/s, the maximum power points are tracked at each wind speed.

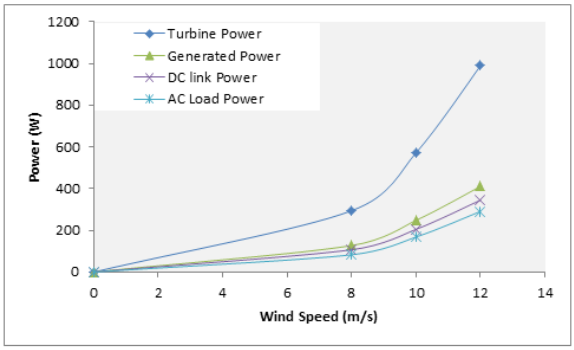

Figure 23 Power at different points of WECS and different wind speeds under MPPT control

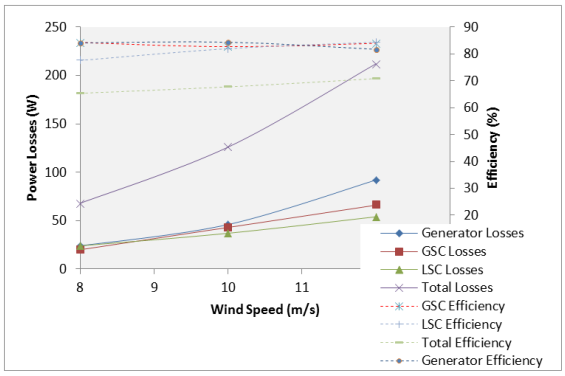

Figure 24 The wind energy conversion system power losses and efficiency at different wind speeds under MPPT control technique

From Figure 23, analysis of losses and efficiency of the wind energy conversions system under investigation can be obtained as shown in Figure 24. As maximum power points are tracked so are the losses as wind speed varies. It can be seen that for this particular WECS, the PMSG contributed the larger portion of the losses with a maximum value of 92W at 12m/s while the generator side inverter generated maximum losses of 66W and the load side inverter generated 54W losses. It is also observed that the efficiency of each of the component and the total system vary slightly as wind speed varies with the system's total efficiency at maximum value of 71% at 12m/s typical of small machines.

International Journal of Engineering Research & Technology (IJERT)
ISSN: 2278-0181
Vol. 5 Issue 12, December-2016

A. Comparison of simulation run time

Table 2: Comparison of simulation run time between switching model and the proposed AVM of full scale back-back VSI with PMSG WECS

Models	Time step	Simulation set time	Time taken to complete simulation
Switching model	$100e^{-9}$	0.5	4.5 hours
Proposed AVM	$30e^{-6}$	0.5	5 minutes

In all the simulations, the step sizes were chosen to reflect the requirements of each method. The limiting factor of the proposed average value model is the minimum step size, which is restricted here to less than the PI control loop run time of 50 microseconds on a typical DSP. For the PWM switching model, the limiting factor is minimum step size, which is set to the resolution of the PWM duty cycle, typically $<1000^{th}$ of PWM switching period. Table 2 shows the comparison of the simulation completion time between switching model and the proposed AVM. It can be seen that with the simulation set time of 0.5s, completion time for the switching model with a time step of $100e^{-9}$ is 4.5 hours while the simulation completion time for the AVM with freedom of time step $30e^{-6}$ is 5 minutes which is 54 times faster than the switching model.

VIII. CONCLUSIONS

In this paper an alternative simulation model and detailed switching model for full scale back-back voltage source inverters with variable speed PMSG WECS has been developed and implemented in PORTUNUS software. The proposed model achieves not only the ability to reproduce the power-speed characteristics, torque-speed characteristics and accurate power transfer from the wind turbine generator to the AC load, but also can accurately implement control technique to track reference current and maximum power points with simulation run time 54 times faster compared to the switching model. Hence, the developed average voltage estimation model can be used for a time scheduled design process performance analysis of power electronic converters, variable speed generators wind energy conversion system and control techniques.

ACKNOWLEDGMENT

We would like to acknowledge Tertiary Education Trust Fund (TETFund), Nigeria and Cross River University of Technology, Nigeria for the funding.

REFERENCES

[1] Shahabi, M. Haghifam, M. -R.; Mohamadian, M. and Nabavi-Niaki, "Microgrid dynamic performance improvement using a doubly fed induction wind generator," IEEE Transactions on Energy Conversion, vol. 24, Issue 1, pp 137-145, March 2009.

[2] Chowdhury, M.M; Haque, M. E.; Gargoom, A. and Negnevitsky, M., "Performance improvement of a grid connected direct drive wind turbine using super-capacitor energy storage," IEEE PES Innovative Smart Grid Technologies (ISGT), Washington, DC, pp 1-6, 24-27 Feb. 2013.

[3] F. Kendouli, K. Abed, K. Nabti and H. Benalla and B. Azoui, "High performance PWM converter control based PMSG for variable speed wind turbine," First International Conference on Renewable Energies and Vehicular Technology (REVET), Hammamet, pp 502-507, 26-28 March 2012

[4] Hui, Joanne, Bakhshai, Alireza and Jain, Praveen, "Power management supervisory control algorithm for standalone wind energy systems," IEEE 36th International Telecommunications Energy Conference (INTELEC), Vancouver, BC, Canada, pp 1-6, Sept. 28, 2014 – Oct. 2, 2014.

[5] Ahmed, S.; Boroyevich, D.; Wang, F. and Burgos, R. "Development of a new voltage source inverter (VSI) average model including low frequency harmonics," Twenty-Fifth Annual IEEE Applied Power Electronics Conference and Exposition (APEC), Palm Springs, CA, pp 881-886, 21-25th Feb. 2010.

[6] Tabarraee, K.; Iyer, J.; Atighechi, H. and Jatskevich, J, "Dynamic average-value modelling of 120^0 VSI-commutated brudhless DC motors with trapezoidal back emf," IEEE Transactions on Energy Conversion, vol. 27, Issue 2, pp. 296-307, June 2012.

[7] Hoff, B. and Sulkowski, W, "Comprehensive modelling and practical verification of grid connected VSI with LCL Filters," 15th International Power Electronics and Motion Control Conference (EPE/PEMC), Novi Sad, DS3f.7-1-DS3f.7-7, 4-6 Sept. 2012.

[8] Yaohua Li, Dieter Gerling and Weiguo Liu, "A Simplified voltage vector selection strategy for the Permanent Magnet Synchronous Motor Direct Torque Control Drive with Low Torque Ripple and Fixed Switching Frequency," International Conference on Electrical Machines and Systems (ICEMS), Incheon, pp 674-679, 10-13 Oct. 2010.

[9] Howlader, A.M, Urasaki, N, Yona, A, Senjyu, T, Saber, A.Y., "An online fuzzy adaptive pulse amplitude modulation control for a PMSM drive," 7th IEEE conference on industrial electronics and applications (ICIEA), Singapore, pp 40-45, 18-20 July 2012.

[10] Yonggao Zhang, Guangjian Kuang and Lizhong Long, "Research on Reduced common-mode voltage nonzero vector Pulse width modulation technique for Three-phase Inverters," 7th International Power Electronics and Motion Control Conference (IPEMC), Harbin, China, vol.4, pp 2349-2352, 2-5 June 2012.

[11] Lazi, J. M.; Ibrahim, Z.; Sulaiman, M.; Jamaludin, I. W. and Lada, M. Y. "Performance Comparison of SVPWM and Hysteresis Current Control for Dual Motor Drives," IEEE Applied Power Electronics Colloquium (IAPEC), Johor Bahru, pp 75-80, 18-19 April 2011.

[12] Yaohua Li, Dieter Gerling and Weiguo Liu, "A Simplified Voltage Vector Selection Strategy for the Permanent Magnet Synchronous Motor Direct Torque Control Drive with Low Torque Ripple and Fixed Switching Frequency," International Conference on Electrical Machines and Systems (ICEMS), Incheon, pp 674-679, 10-13 Oct. 2010.

[13] Pasi Nuutinen, Aleksi Mattsson, Tero Kaipia, Pasi Peltoniemi, Antti Pinomaa, Andrey Lana, Janne Karppanen and Pertti Silventoinen, "Power Electronic Losses of a Customer-end Inverter in Low-Voltage Direct Current Distribution," 16th European Conference on Power Electronics and Applications (EPE'14-ECCE Europe), Lappeenranta, pp 1-10 26-28 Aug. 2014.

[14] Muyeen, S. M. and Al-Durra, A, "Modeling and control strategies of fuzzy logic controlled inverter system for grid interconnected variable speed wind generator," IEEE System Journal, vol. 7, No. 4, pp 817-824, Dec. 2013.

[15] Wei Qiao Xu Yang and Xiang Gong, "Wind Speed and Rotor Position Sensorless Control for Direct-Drive PMG Wind Turbines, IEEE Transactions on Industry Applications, vol 48, Issue 1, pp 3-11, Jan. –Feb. 2012.

International Journal of Engineering Research & Technology (IJERT)
ISSN: 2278-0181
Vol. 5 Issue 12, December-2016

[16] Daniel A. F. Collier and Marcelo L. Heldwein, "Modeling and design of a micro wind energy system with a variable-speed wind turbine connected to a permanent magnet synchronous generator and a PWM rectifier," Brazilian Power Electronics Conference (COBEP), Praiamar, pp 292-299, 11-15 Sept. 2011.

[17] Errami, Y.; Benchagra, M.; Hilal, M.; Maaroufi, M. and Quassaid, M., "Control strategy for PMSG wind farm based on MPPT and direct power control," International Conference on Multimedia Computing and Systems (ICMCS), Tangier, pp 1125-1130, 10-12 May 2012.

Appendix

Table 3 Parameters of PMSG

Rated power	1kW
No. of poles	16
Stator resistance	0.2 Ohms
D-axis Inductance	4mH
Q-axis Inductance	4mH
Flux linkage	0.075 Vs
Moment of inertia	0.1

Table 4 Parameters of wind turbine

Rated power	1kW
No. of rotor blade	5
Rotor diameter	2m
Rated wind speed	12m/s
Cut- in wind speed	2m/s